Strasbourg (France)

MANUSCRIPT COVER PAGE FORM

E-MRS Symposium : G – Functional Materials for Micro and Nano Systems
Paper Number : G 10 03
Title of Paper : Defect study in SnO_2 by cathodoluminescence analysis

Corresponding Author : J. Daniel Prades García

Full Mailing Address : Facultat de Física – Departament d'Electrònica
Martí i Franquès,1
08028 – Barcelona
SPAIN

Telephone : +34 93 40 39 147
Fax : + 34 93 40 21 148
E-mail: dprades@el.ub.es

Defect study of SnO_2 nanostructures by cathodoluminescence analysis: application to nanowires

J.D. Prades[1], J. Arbiol[1,2], A. Cirera[1], J.R. Morante[1], M. Avella[3], L. Zanotti[4], E. Comini[5], G. Faglia[5], G. Sberveglieri[5]

[1] EME/CeRMAE/IN^{2}UB, Dept. d'Electrònica, Universitat de Barcelona, C/ Martí i Franquès, 1, E-08028 Barcelona, Spain
[2] TEM-MAT, Serveis Cientificotècnics, Universitat de Barcelona, C/ Martí i Franques 1, E-08028, Barcelona, Spain
[3] Departamento Física de la Materia Condensada, Universidad de Valladolid. Paseo de la Magdalena s/n Valladolid, Spain.
[4] IMEM-CNR, Parco Area delle Scienze 37/A, 43010 Fontanini, Parma, Italy
[5] Sensor Lab., INFM, Brescia University, Via Valotti 9, 25133 Brescia, Italy.

Abstract:

Defects in SnO_2 nanowires have been studied by cathodoluminescence, and the obtained spectra have been compared with those measured on SnO_2 nanocrystals of different sizes in order to reveal information about point defects not determined by other characterization techniques. Dependence of the luminescence bands on the thermal treatment temperatures and pre-treatment conditions have been determined pointing out their possible relation, due to the used treatment conditions, with the oxygen vacancy concentration. To explain these cathodoluminescence spectra and their behavior, a model based on first-principles calculations of the surface oxygen vacancies in the different crystallographic directions is proposed for corroborating the existence of surface state bands localized at energy values compatible with the found cathodoluminescence bands and with the gas sensing mechanisms. CL bands centered at 1.90 eV and 2.20 eV are attributed to the surface oxygen vacancies 100º coordinated with tin atoms whereas CL bands centered at 2.37 eV and 2.75 eV are related to the surface oxygen vacancies 130º coordinated. This combined process of cathodoluminescence and ab initio calculations is shown to be a powerful tool for nanowire defect analysis.

Key words:

SnO_2, CATHODOLUMINESCENCE, NANOSTRUCTURE, NANOWIRE, OXYGEN VACANCY, AB INITIO

1.- Introduction:

Tin dioxide (SnO_2) plays a key role in solid state gas sensors [1]. So a lot of experimental work has been done in order to characterize SnO_2 not only from the technological point of view as a sensor of different gases [2] but also from the materials science standpoint [3] so as to achieve improved performances by means of a better knowledge of the synthesized materials. The vacancy defects investigation deserves special attention as they have been clearly related to conductive and sensing properties of metal oxides [2]. This article will deal with the analysis of point defects using cathodoluminescence (CL) spectra of nanostructured SnO_2, as this technique reveals complementary information about radiative transitions related to these point defects that is not determined by other characterization techniques

This experimental procedure is not new. Since the mid-1970s, however, few works have been published presenting the CL spectra of SnO_2 with different morphologies [4,5,6,7]. In all known cases, several bands between 1.9 and 2.6eV have been reported but there still remains some uncertainty on their origin [6]. However, there are no systematic and detailed works considering nanowires and their comparison with nanoparticles of different sizes.

On the other hand, first-principles methodologies based on the density functional theory (DFT) now provide precise calculations of the energetic properties of bulk materials and their surfaces in moderate computing times [8]. Consequently, it is attractive to link theoretical findings with unclearly interpreted experimental results in order to attain better materials knowledge with a straightforward technological application such as a fast and low cost defect detection.

The aim of this article is to show how CL, with its notable spatial resolution, can be methodologically combined with the ab initio calculation and applied to analyze the role played by the surface oxygen vacancy defects in nanostructured SnO_2.

First, data from the literature about intra-gap energy levels and new DFT calculations are reported and discussed. Second, CL spectra of liquid pyrolysis synthesized SnO_2 nanoparticles with different grain sizes are presented and four different bands are identified. On the basis of these experimental results, a model is proposed. Finally, this model is applied to the surface oxygen vacancy defect detection of two different samples of SnO_2 nanowires.

2.- Experimental details:

The cathodoluminescence measurements (CL) were carried out in a Gatan XiCLone system attached to a JEOL JSM-820 scanning electron microscope. The collected luminescence was analyzed by a 300-line grating monochromator and detected by a Peltier cooled CCD, whose spectral range covers [200,1200]nm (around [6.2,1.0]eV). The CCD records the whole spectrum at once in the selected spectral window, thus reducing the measuring times. The system is equipped with a cryostat that allows low temperature measurements.

The measurements were carried out at liquid nitrogen temperature (~ 80K). The excitation beam conditions for the SnO_2 powders were 20kV for accelerating voltage and ~40nA for beam current. The nanowires were measured with an accelerating voltage of 10kV and a beam current of approximately ~5nA. Details on sample synthesis are given below.

The structural and morphological characterization of some of our samples was carried out by means of transmission electron microscopy (TEM) and selected area electron diffraction (SAED). In order to obtain the high-resolution TEM (HRTEM) results we used a Jeol 2010F field emission gun microscope, which works at 200kV and has a point-to-point resolution of 0.19nm. To improve the contrast and resolution of our images, minimizing the chromatic aberration inherent in HRTEM micrographs, we obtained the images by filtering the electron zero loss peak, using a Gatan Image Filter (GIF 2000).

3.- Results and discussion:

3.1- Intra-gap energy levels of SnO_2:

For SnO_2, it is established the abundance of shallow donor levels mainly located between 0.15 and 0.30eV below the conduction band minimum (CBM). Henceforth, we will refer to those levels as bulk shallow levels. According to electro-physical study data, ionized oxygen vacancies in tin dioxide form shallow donor levels with an energy of ~0.03 and ~0.15eV below the bottom of the CBM [9,10,11]. In electron spin resonance measurements, other authors have observed the existence of donor levels from ~0.15eV up to ~0.30eV underneath the CBM [12]. Note that the literature only shows how, for a given

sample, one (or several) discreet levels are placed around this 0.15eV broad energy region but does not suggest the existence of a continuous band 0.15eV wide. In what follows, the level at ~0.03eV will not be considered as long as it is indistinguishable from the CBM with the computational techniques and the experimental results shown below. In terms of luminescence, the existence of these bulk shallow levels means that when a SnO_2 sample is excited not only the very bottom states of the CBM but also the bulk shallow levels are populated, all those levels being the initial possible states of an eventual radiative recombination.

As far as the surface is concerned, there is much less previous data in the literature. However, these surface defects are relevant in determining the gas sensing mechanisms, especially in tiny nanostructured materials where the surface characteristics stand out clearly. Initially, we will center the discussion on the (110) surface that is considered the most common faceting orientation [13]. Figure 1 shows the atomic arrangement on the SnO_2-cassiterite (110). A striking feature of this surface is the presence of so-called 'bridging' oxygen atoms (O_{Bridg}). These coordinate with their first neighboring tin atoms, forming an angle of 100º. It has been observed that simple heating of a stoichiometric SnO_2-cassiterite (110) surface to temperatures above 225ºC leads to loss of O_{Bridg} and the formation of oxygen bridging vacancies ($O_{BridgVac}$) [14,15]. According to the literature, if the temperature is raised above 525ºC, in-plane oxygen vacancies ($O_{InPlaneVac}$) can be formed [14]. Such a vacancy coordinates with neighboring Sn atoms forming an angle of 130º. It is worth noting that, as stated in [14], the given vacancy generation temperatures may be dependent on the particular samples used.

At this point, we recall that real samples are not only faceted with (110) surfaces; therefore, a plethora of different oxygen vacancy sites over different surface orientations arise. In fact, deeper analysis shows that there are only two relevant surface oxygen vacant configurations: those that coordinate and form and angle of 100º ($O_{BridgVac}$ in the case of the (110) surface) and those of 130º ($O_{InPlaneVac}$). In order to investigate the band structure consequences of the surface vacancies formation ab initio, calculations of several low index surfaces of SnO_2-casiterite were performed.

The first-principles methodology used in the present calculations is based on the density functional theory [16,17] (DFT) as implemented in the SIESTA code [18,19]. We make use of the generalized gradient approximation (GGA) for the exchange-correlation functional [20]. For all atomic species double

ζ plus polarization orbital basis-sets were used. Total energy convergence is guaranteed below 10meV as is usual in this kind of calculations [21]. A real space mesh cut-off of 250Ry and a reciprocal space grid cut-off of approximately 15Å were used. The structural relaxations were done by means of a conjugate gradient minimization of the energy, until the forces on all the atoms were smaller than 0.04eV/Å (which provides relaxed total energy values more stable than 10meV). No constraints were imposed on the relaxation where the forces were calculated as analytical derivatives of the total energy [22]. The convergence of the present results was verified for slabs thicker that 2 stoichiometric layers, 2x1 bulk unit cells wide, and with 7Å of vacuum spacing.

The initially considered low-index orientations are (110), (100), (101) and (001), which are accepted as some of the most common faceting surfaces of SnO_2-cassiterite [13]. It is worth noting that 100º coordinated oxygens are present on (110) and (100) surfaces and 130º coordinated oxygens appear in surfaces (110), (101) and (001). For all these cases, electron densities of states were computed for stoichiometric and reduced surface (i.e. without and with the oxygen vacancy). In all cases, the vacancy formation implies the creation of allowed states near the top of the valence band (energetic positions are given in Table 1). In summary, it is clear that two families of levels appear: one due to a 100º coordinated vacancy at approximately 1.40eV above the valence band and a second, due to 130º coordinated, at 0.90eV. Finally, it is worth pointing out that this description in terms of coordination angles seems general enough to describe the rich surface vacancies casuistic, independently on the surface orientation (or the particle morphology).

3.2.- Nanocrystalline powder CL spectrum:

Figure 2 shows the acquired CL spectra obtained using samples of SnO_2-cassiterite nanocrystalline particles prepared by liquid pyrolysis. This synthesis technique involves thermal treatment of a microdrop of tin chloride solution deposited onto a polished substrate [23]. Samples analyzed in this study were treated for 24 minutes at stabilization temperatures ranging from 300 to 1000ºC. More details on this particular samples synthesis and characterization can be found in reference [24].

Table 2 presents the corresponding fitting data of the CL spectra. It is a remarkable feature that the CL signal increases with the treatment temperature. According to these results, it is possible to identify four

different contributions centered at 1.90eV, 2.20eV, 2.37eV and 2.75eV. The two lower energy bands appear in all samples whereas the two higher ones emerge at temperatures above 700ºC (see Figure 3).

In light of the theoretical vacancy analysis presented above and the SnO_2 experimental spectra evolution, it is possible to sketch a fairly simple model. Figure 4 shows schematically the energetic intra-gap positions of the bulk shallow levels and the two kinds of surface oxygen vacancies (100º and 130º coordinated). According to this, the four recombinations from conduction band and bulk shallow levels to the surface vacancy levels would arise four mean energy values compatible with the bands found experimentally within the computational accuracy (±0.05eV): 1.98eV, 2.20eV, 2.48eV and 2.70eV.

Linking these four bands with their contribution to the spectra as a function of the sample treatment temperature, one could propose that 1) bulk shallow levels are present at all temperatures as long as their energy level is the origin of the recombination of at least one band (1.90 eV) in all samples; 2) at lower temperatures, 100º coordinated oxygen vacancies are present whereas the apparition of 130º oxygen vacancies begins above 700ºC.

Regarding the first proposal, it is worth noting that, as discussed above, bulk shallow levels are commonly present in SnO_2 in the studied range of treatment temperatures (this is, for example, the case of bulk oxygen vacancies).

Finally, and concerning the second proposal, it is congruent with the vacancy formation evolution previously described where 130º coordinated vacancies are harder to generate by heating than the 100º coordinated ones. In this sense, it should be remarked that, based only on a particular set of samples, strongly setting a fixed threshold temperature for the production of one kind of surface vacancy or another seems difficult.

3.3.- Nanowires CL spectrum:

Unlike nanoparticles, nanowires present better defined crystallographic surfaces and, depending on their geometric dimensions, the role played by surface oxygen vacancies becomes more essential for determining their electrical characteristics as well as their gas sensing mechanisms. Therefore, for understanding the nanowire properties and their applications as gas nanosensors, it is also basic to verify

the role of these oxygen surface vacancies. In this context, the previous experimental and analytical procedure was also applied to different SnO_2 nanowires with different surface oxygen vacancy configuration.

The deposition of SnO_2 nanowires was performed in a tubular furnace with either quartz or alumina tubes. The deposition system was equipped with a vacuum pump in order to obtain a pressure lower than 1mbar, and mass flow controllers in order to inject a controllable amount of gas carrier during the deposition.

Two different deposition procedures were pursued. In the first one (A-type nanowires), tin monoxide was used as source material, allowing lower working temperatures. Tin monoxide is placed at the center of the quartz tube and the alumina substrates are positioned in the lower temperature region; then, the system is pumped and the temperature is raised to 300°C in vacuum. A subsequent temperature ramp to 900°C is imparted, keeping a 100sccm flux of Ar/H_2 at 300mbar in order to prevent the oxidation of tin monoxide. At temperatures higher than 750°C, the dissociation of tin monoxide into tin and tin dioxide takes place and leads to a complete dissociation. The carrier gas transports tin vapors and, due to the lower temperature of the substrates, there is a condensation in liquid droplets with dimensions ranging from tens of nanometers to microns. The temperature is then slowly decreased to 870°C and an Ar/O_2 flux is introduced. Oxygen reacts with tin droplets and forms SnO_2 nuclei, which then develop in elongated nanocrystals. Finally the system is cooled to room temperature.

For the second deposition procedure (B-type nanowires), tin dioxide powder was used as source material: tin dioxide is place at the center of the alumina tube at 1370°C and a flux of 75sccm of Ar is used as gas carrier at a pressure of 100mbar. Tin oxide nanowires are collected at temperatures ranging from 430 to 470°C.

Notice that whereas A-type nanowires are finally grown and collected at temperatures above 700ºC, B-type nanowires are collected at temperatures around 450ºC. These final thermal conditions determine the final surface vacancy configuration of the wires.

The presented nanowires were observed with SEM and TEM. A-type samples present nanostructures with widths ranging from 20 to 200nm, while lengths of up to 200µm are found. The example micrograph shown in Figure 5.a was captured by means of bright-field TEM (BFTEM). At this point we obtained selected area electron diffraction (SAED) patterns from several nanowire-like structures in order to determine their structural composition. A SAED example is shown in Figure 5.b, corresponding to the diffraction pattern obtained on the squared area in Figure 5.a. A priori, SAED results confirmed our previous X-ray diffraction (XRD) analysis where a clear SnO_2 cassiterite ($P4_2$-mnm) structure seemed to be mainly present in our samples. As regards B-type sample, it presents well-formed wire structures with widths from 50 to 1500 nm and lengths of over 100µm. Figure 6 shows a representative SEM view. By means of HRTEM we found that the SnO_2 cassiterite nanowires observed in sample A mainly grow along the [101] direction, with lateral facets defining a square prism corresponding to {010} and {10-1} planes. However, in the case of B samples, we found that the SnO_2 cassiterite nanowires crystallize along the [010] direction while the lateral most favorable facets, attending to HRTEM analysis, are the {200}, {101} and {10-1}, defining a hexagonal prism morphology. Nevertheless, both structures differ from those Pd doped SnO_2 cassiterite nanowire-like structures reported previously [25], which grew along the [001] direction, and had a square prism morphology with {110} and {1-10} lateral facets.

CL spectra of both kinds of SnO_2 nanowires are shown in Figure 7, while fitting values are presented in Table 3. Notably, both CL spectra somehow present a mixture of the four previously presented CL emissive bands. Comparing both spectra, it is remarkable that B-type sample (450ºC) exhibits a clearly higher CL emission with contributions of four bands whereas A-type sample (700ºC) only shows contributions of the higher energy bands. According to the previously described model, these experimental facts can be understood as follows: 1) both samples seem to present bulk shallow levels; 2) B-type sample may contain both kinds of surface oxygen vacancies, whereas A-type sample only shows evidence of 130º coordinated oxygen vacancies.

Remarkably, the fact that it is mainly A-type nanowires that present the hardest to produce kind of vacancies (130ºC coordinated), whereas B-type nanowires present a dominant contribution of 100º coordinated vacancies, seems compatible with the final synthesis temperatures of both samples. As

mentioned before, a fixed, well-defined temperature threshold for the production of one kind of vacancy or the other seems hard to establish, since it is strongly related to the experimental synthesis and thermal treatment procedures.

4.- Conclusions:

A model based on first-principles calculations was proposed to explain the catadoluminescence spectra obtained using nanocrystalline SnO_2 powders treated at different temperatures and using different nanowires. According to this, four experimental bands centered at 1.90eV, 2.20eV, 2.37eV and 2.75eV were identified and related to recombinations from the conduction band and bulk shallow levels to levels near the top of the valence band corresponding to surface oxygen vacancies (100º and 130º tin atoms coordinated). Significant difference in the energy formation of both types of surface oxygen vacancies explains the appearance of these bands. Whereas 100º tin coordinated oxygen surface vacancy is related to 1.90 eV and 2.20 eV bands; the 130º tin coordinated oxygen surface vacancy is related to 2.37 eV and 2.70 eV bands. This appears to be significant in the gas interaction mechanisms and, hence, in the gas sensor performances of these nanostructured materials.

Acknowledgements:

The authors wish to thank Prof. J .Jiménez (Universidad de Valladolid, Spain) for the enlightening discussions and Dr. J.M. Pruneda and Prof. P. Ordejón (ICMAB-CSIC, Spain) for their help in the first steps of the ab initio calculations. This work was partially funded by the European Integrated Project NANOS4 (MMP4-CT-2003-001528) and the Spanish CICyT project MAGASENS. The calculations were partially performed at the facilities of the Supercomputation Center of Catalonia. Finally, J.D. Prades acknowledges the support of the FPU program of the Spanish Ministry of Education and Science.

References:

[1] W. Göpel and K.D.Schierbaum, SnO_2 sensors: current status and future prospects, Sensors and Actuators B, Chemical, 26-27 (1995) 1-12.

[2] G. Sverveglieri, Recent developments in semiconducting thin-film gas sensors, Sensors and Actuators B, Chemical, 23 (1995) 103-109.

[3] M. Batzill and U. Diebold, The surface and materials science of tin oxide, Progress in Surface Science., 79 (2005) 47-154.

[4] D.F. Crabtree, Cathodoluminescence of tin oxide doped with europium, J. Phys. D, 7 (1974) L17-L21.

[5] D.F. Crabtree, Cathodoluminescence of tin oxide doped with terbium, J. Phys. D, 7 (1974) L22-L26.

[6] D. Maestre, A. Cremades and J. Piqueras, Cathodoluminescence of defects in sintered tin oxide, J. Appl. Phys., 95 (2004) 3027-3030.

[7] D. Maestre, A. Cremades and J. Piqueras, Growth and luminescence properties of micro- and nanotubes in sintered tin oxide, J. Appl. Phys., 97 (2005) 044316 (4 pages).

[8] D. Sanchez-Portal, P. Ordejon and E. Canadell, Computing the properties of materials from first principles with SIESTA, Structure and Bonding, 113 (2004) 103-170.

[9] Y.S. He, J.C. Campbell, R.C. Murphey, N.F. Arendt and J.S. Swinnea, Electrical and optical characterization of $SbSnO_2$, Journal of Materials Research, 8 (1993) 3131-3134.

[10] S. Samson and C.G. Fonstad, Defect structure and electronic donor levels in stannic oxide crystals, J. Appl. Phys., 44 (1973) 4618-4621.

[11] C.G.Fonstad and K.H.Rediker, Electrical properties of high-quality stannic oxide crystals, J. Appl. Phys., 42 (1971) 2911-2918.

[12] Y. Mizokawa and S. Nakamura, ESR and electric conductance studies of the fine-powdered SnO_2, Jpn. J. Appl. Phys., 14 (1975) 779-804.

[13] J. Oviedo and M.J. Gillan, Energetics and structure of stoichiometric SnO_2 surfaces studied by first-principles calculations, Surf. Sci., 463 (2000) 93-101.

[14] D.F. Cox, T.B. Fryberger and S. Semancik, Oxygen vacancies and defect electronic states on the SnO_2(110)-1×1 surface, Phys. Rev. B 38 (1988) 2072-2083.

[15] D.F. Cox, T.B. Fryberger and S. Semancik, Preferential isotopic labeling of lattice oxygen positions on the SnO_2(110) surface, Surf. Sci., 227 (1990) L105-L108.

[16] P. Hohenberg and W. Kohn, Inhomogeneous electron gas, Phys. Rev., 136 (1964) B864-B871.

[17] W. Kohn and L.J. Sham, Self-consistent equations including exchange and correlation effects, Phys. Rev., 140 (1965) A1133-A1138.

[18] P. Ordejón, E. Artacho, and J.M. Soler, Self-consistent order-N density-functional calculations for very large systems, Phys. Rev. B, 53 (1996) R10441-R10444.

[19] J.M. Soler, E. Artacho, J.D. Gale, A. García, J. Junquera, P. Ordejón and D. Sánchez-Portal, The SIESTA method for ab initio order-N materials simulation, J. Phys: Condens Matter, 14 (2002) 2745-2779.

[20] J.P. Perdew, K. Burke and M. Ernzerhof, Generalized Gradient Approximation made simple, Phys. Rev. Lett., 77 (1996) 3865-3868.

[21] J. Oviedo and M.J. Gillan, First-principles study of the interaction of oxygen with the SnO_2(110) surface, Surf. Sci., 490 (2001) 221-236.

[22] D. Sánchez-Portal, P. Ordejón, E. Artacho, J. M. Soler, Density-functional method for very large systems with LCAO basis sets, Int. J. Quantum Chem., 65 (1997) 453-461.

[23] A. Cirera, A. Diéguez, R. Diaz, A. Cornet, J.R. Morante, Proceedings of Eurosensors XII, Southampton, UK, Sensors and Actuators B, 58 (1999) 360.

[24] A. Cirera, A. Cornet, J. R. Morante, S. M. Olaizola, E. Castaño and J. Gracia, Comparative structural study between sputtered and liquid pyrolysis nanocrystaline SnO_2, Mat. Sci. and Eng. B, 69-70 (2000) 406-410.

[25] J. Arbiol, A. Cirera, F. Peiró, A. Cornet, J. R. Morante, J. J. Delgado and J. J. Calvino, Optimization of tin dioxide nanosticks faceting for the improvement of palladium nanocluster epitaxy, Applied Physics Letters, 80 (2002) 329-331.

Biography:

J. Daniel Prades: graduated in Physics at the University of Barcelona in 2005. Now he is PhD student in Department of Electronics of the same university. His current research is focused on first-principles modeling of electronic and vibrational properties of nanostructured metal oxides.

Dr. Jordi Arbiol: graduated in Physics at the University of Barcelona in 1997 received his European PhD in Physics in 2001, and obtained the PhD Extraordinary Award of the Electronics Department. He joined the Electronics Department in 1997, and in 2000 he was appointed as Assistant Professor in this department. His current research activities are centered in the structural, compositional and morphological characterization of nanosized materials and devices by means of TEM related techniques (HRTEM, EELS, EFTEM, Z-contrast, Electron Tomography).

Dr. Albert Cirera: graduated in Physics at the University of Barcelona in 1996. He received his PhD in 2000 from the University of Barcelona, developing new technologies and their characterization for tin oxide gas sensor devices. He is currently associate professor and works in the field of sensors and its simulation, as scientist and coordinator in several related industrial projects.

Prof. Dr. Joan R. Morante: was born in Mataró (Spain). At 1980 he received the Ph D degree in Physics from the University of Barcelona. Since 1986 he is full professor of Electronics and director of the Electronic Materials and Engineering, EME, group. He has been dean of the Physics Faculty and academic advisor of the Electronic Engineering degree. He was director of the Electronics Department in the University of Barcelona which is associated unity to the Centre Nacional de Microelectronics at Bellaterra (Barcelona). Actually, he is research head of the EME group and co-director of the CEMIC, center of the Microsystems Engineering and director of the CeRMAE, reference center of advanced materials for energy from Generalitat of Catalunya. His activity is devoted to the electronic materials and technology, physics and chemical sensors, actuators, and microsystems. He has especial interest in nanoscience and micro&nanotechnologies. He has collaborated in international R&D projects as BRITE, GROWTH (micromechanics, microengineering, gas sensors, nanomaterials...), ESPRIT, IST (advanced devices,

sensors, actuators, microsystems, electronic systems,...), JOULE,...EUREKA, IBEROEKA and industrial projects. He is co-author of more than 400 works in international specialized journal and member of international committees and editorial boards in the field of electronic materials and technology, sensors&actuators and microsystems, and electronic systems. He has been distinguished with the research prize Narciso Monturiol and the "senior research distinction" award from the Generalitat of Catalunya (Spain) .

Dr. Manuel Avella: graduated and obtained his PhD in 2000 at the Universidad de Valladolid, Spain. He belongs to the research staff of the Dpt. Fisica Materia Condensada. In 1992, he started his research in this department, collaborating in the development of an equipment of Spatially Resolved Photocurrent for semi-insulating InP:Fe characterization. He is currently involved in the Scanning Electron Microscopy (SEM) and Cathodoluminescence (CL) measurements for characterization on semiconductor materials (GaAs, ZnO, InP, ternary and quaternary alloys, ...) and devices (laser diodes, photonic crystals...). He is also skilled to work with other additional techniques, such as micro-Raman Spectroscopy, AFM, EDS X-ray Microanalysis and Phase Stepping Microscopy (PSM). He has participated in more than 12 international research projects and industry contracts. The scientific results were published in more than 60 papers in international journals and over 50 international conferences.

Dr. Lucio Zanotti: was born on 15th July 1944. He has been graduated from the University of Bologna in 1969 with a specialization in chemistry. He is one of the founders of MASPEC Institute of the Italian National Council of Research and has been working there since 1970. Since 1983 he is head of the Technology Department at MASPEC. His research has been carried out mainly in the field of semiconductor compounds for use in micro and opto-electronics, infrared detectors and photovoltaic cells and in the field of inorganic/organic materials for non-linear optical application. His activity has been centered around: inorganic synthesis, purification procedures, impurity and compositional-inhomogeneity analysis, crystal growth of binary, ternary and multinary compounds from the melt, vapor and solution,

defect (chemical etching) analysis, electrical and optical characterization. He is director of MASPEC (presently IMEM Institute) since 1987, is author of well over 150 scientific papers, reviews, patents in the field of material science and technology.

Dr. Elisabetta Comini: was born on November 21st, 1972 and she received her degree in Physics at the University of Pisa in 1996. She received her PhD in material science at the University of Brescia. She is presently working on chemical sensors with particular reference to deposition of thin films by PVD technique and electrical characterisation of MOS thin films. In 2001 she has been appointed assistant professor at the University of Brescia.

Prof. Dr. Guido Faglia: was born in 1965 and has received an M.S. degree from the Polytechnic of Milan in 1991 with a thesis on gas sensors. In 1992, he has been appointed as a researcher by the Thin Film Lab at the University of Brescia. He is involved in the study of the interactions between gases and semiconductor surfaces and in gas sensors electrical characterization. In 1996, he has received the Ph.D. degree by discussing a thesis on semiconductor gas sensors. In 2000, he has been appointed as associate professor in experimental physics at University of Brescia. During his career, Guido Faglia has published more than 50 articles on International Journals with referee.

Prof. Dr. Giorgio Sberveglieri: was born on 17th July 1947, and received his degree in Physics from the University of Parma, where, starting in 1971, his research activities on the preparation of semiconducting thin film solar cells was conducted. He has been appointed as the Associate Professor at the University of Brescia in 1987. In the following year, he established the Thin Film Laboratory afterwards called Gas Sensor Laboratory, which is mainly devoted to the preparation and characterization of thin film chemical sensors. He has been the Director of the GSL since 1988. In 1994, he was appointed as full Professor in Physics, first at the Faculty of Engineering of University of Ferrara and then in 1996, at the Faculty of Engineering of University of Brescia. He is a referee of the journals Thin Solid Films, Sensors and Actuators, Sensors and Materials, etc., and is a member of the Scientific Committee of Conferences on Sensor and Materials Science. During his 25 years of scientific activities, Giorgio Sberveglieri has

published more than 140 papers on international reviews; he has presented more than 50 Oral Communications to international congresses and numerous oral communications to national congresses.

Tables:

Table 1: Ab initio results of oxygen vacancy levels over the top of the valence band. The computational accuracy was established to be better than 0.05eV. Consequently, the presented results arise with two families of solutions with average values approximately 1.40eV and 0.90eV above maximum valence band.

Surface	**Sn-coordination angle [°]**	**$O_{vacancy}$ energy level over valence band [eV]** (±0.05)
(110)	100 (Bridging)	1.38
	130 (In Plane)	0.94
(100)	100	1.42
(101)	130	0.86
(001)	130	0.90

Table 2: Gaussian deconvolution parameters of the spectra shown in Figure 2. Notice that these results reveal the existence of four different bands at approximately 1.90eV, 2.20eV, 2.37eV and 2.75eV. Also observe that the two higher energy bands only appear at temperatures above 700ºC. Gains sizes estimated by XRD analysis corroborated by TEM observation are given when available.

Temperature [ºC]	**Grain size [nm]**	**Center [eV]**	**FWHM [eV]**	**Height [a.u.]**
1000	46.7	*2.76*	*0.28*	*0.21*
		2.37	*0.37*	*1.00*
		2.19	0.38	0.70
		1.87	0.22	0.38
800	22.9	*2.74*	*0.26*	*0.10*
		2.38	*0.34*	*0.50*
		2.20	0.35	0.36
		1.87	0.23	0.14
700	16.9	2.19	0.50	*0.38*
		1.90	0.21	*0.12*
500	8.4	2.20	0.46	*0.32*
		1.87	0.29	*0.10*
400	7.0	2.21	0.46	*0.24*
		1.89	0.23	*0.07*
300	–	2.18	0.46	*0.06*
		1.94	0.21	*0.01*

Table 3: Gaussian deconvolution parameters of the spectra shown in Figure 7. Notice that for B-type sample it was possible to identify contributions of the four identified bands, whereas in the A-type sample only contributions of the two bands possibly related to 130º coordinated oxygen vacancies were detected.

Sample	**Center [eV]**	**FWHM [eV]**	**Height [a.u.]**
B-type	*2.72*	*0.31*	*0.35*
	2.38	*0.29*	*0.67*
	2.17	0.27	1.00
	1.95	0.18	0.47
A-type	*2.76*	*0.20*	*1.00*
	2.42	*0.46*	*0.54*

Figure Captions:

Figure 1: SnO_2-cassiterite (110) surface model. Most relevant atoms are indicated. Note how $O_{Bridging}$ coordinates form a 100º angle with six-fold coordinated tin atoms (Sn_{6c}) while $O_{InPlane}$ forms a different angle of 130º with Sn_{5c} and Sn_{6c}.

Figure 2: CL spectra of SnO_2 nanocrystalline particles thermally treated at temperatures ranging from 300ºC to 1000ºC. All spectra were acquired under the same experimental conditions: acceleration voltage of 20kV and beam current of ~40nA with the sample cooled at ~80K. It is remarkable how emission increases with the sample treatment temperature. The approximate centers of the four fitted bands are shown; fitting details are given in Table 2.

Figure 3: Evolution with the sample thermal treatment temperature of the intensity of the four peaks fitted to the spectra shown in Figure 2 (numerical values are given in Table 2). Remarkably, there is a general tendency that shows an increase of all contributions with the treatment temperature. Besides, the increase is even stronger for temperatures above 700ºC appearing two new contributions at 2.37 and 2.75eV.

Figure 4: Schematic representation of the intra-gap levels of SnO_2 corresponding to bulk shallow levels and oxygen surface vacancies. For clarity, energy zero was set at the top of the valence band. Recombinations compatible with the acquired CL spectra are shown. In the case of recombinations from bulk shallow levels (which are located within a 0.15eV wide energy region) the two extreme values are given. From now on, we will consider the average values of the four proposed transitions: 2.70, 2.48, 2.20 and 1.98eV but keeping in mind the uncertainty in the energy of shallow levels. It is also worth remembering that the computational accuracy of the oxygen surface vacancy levels was estimated at ±0.05eV.

Figure 5: a) General bright field TEM view of the SnO_2 A-type nanowires. b) SAED pattern of the area squared in orange in Figure 5.a.

Figure 6: General SEM view of the B-type sample. Inset: detail SEM view of the same sample.

Figure 7: CL spectra of SnO_2 nanowires synthesized with two different methods. All spectra were acquired under the same experimental conditions: accelerating voltage of 10kV and beam current of ~5nA with the sample cooled at ~80K. The approximate centers of the four fitted bands are shown; fitting details are given in Table 3.

Figure 1

Click here to download high resolution image

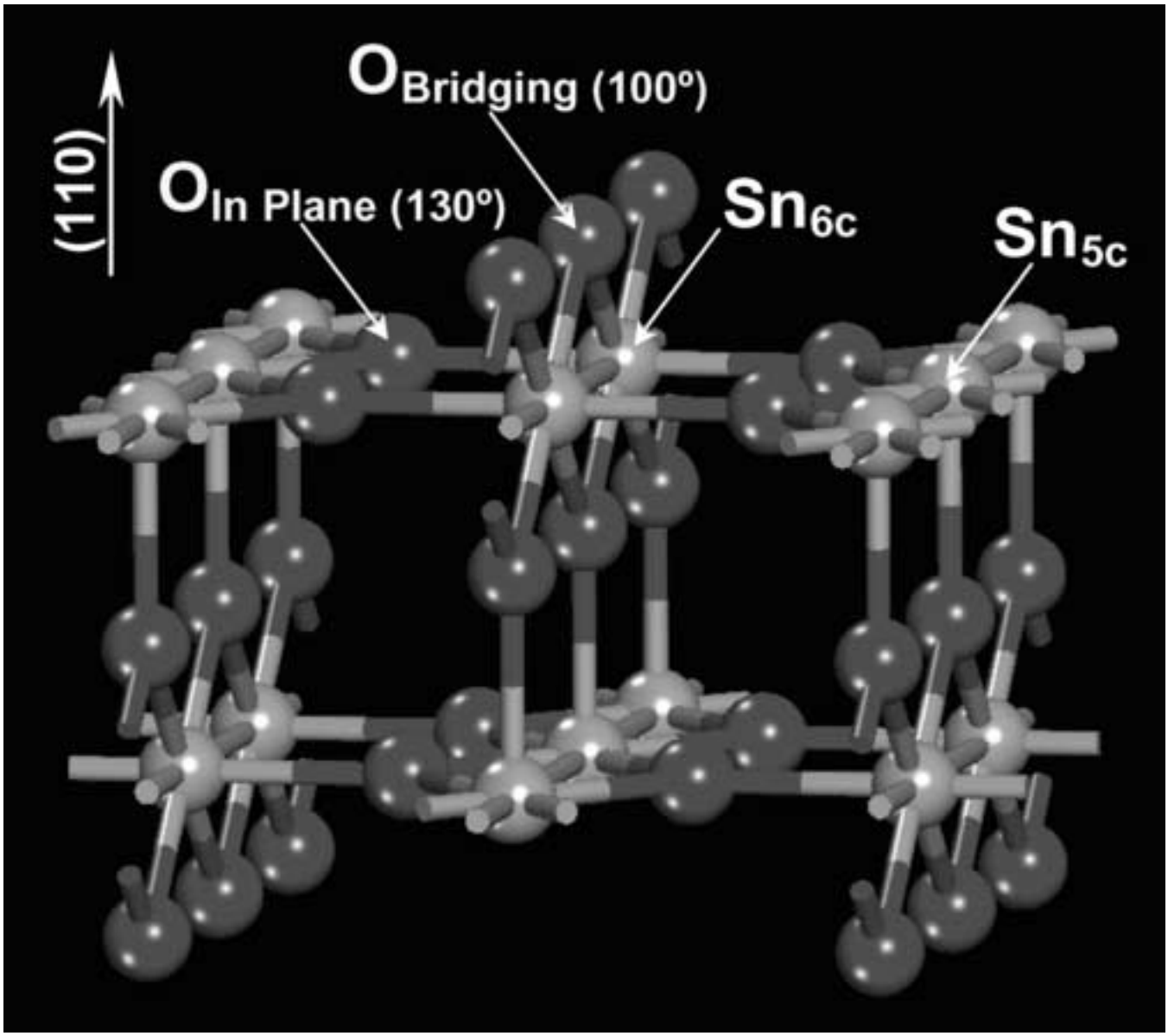

Figure 2

Click here to download high resolution image

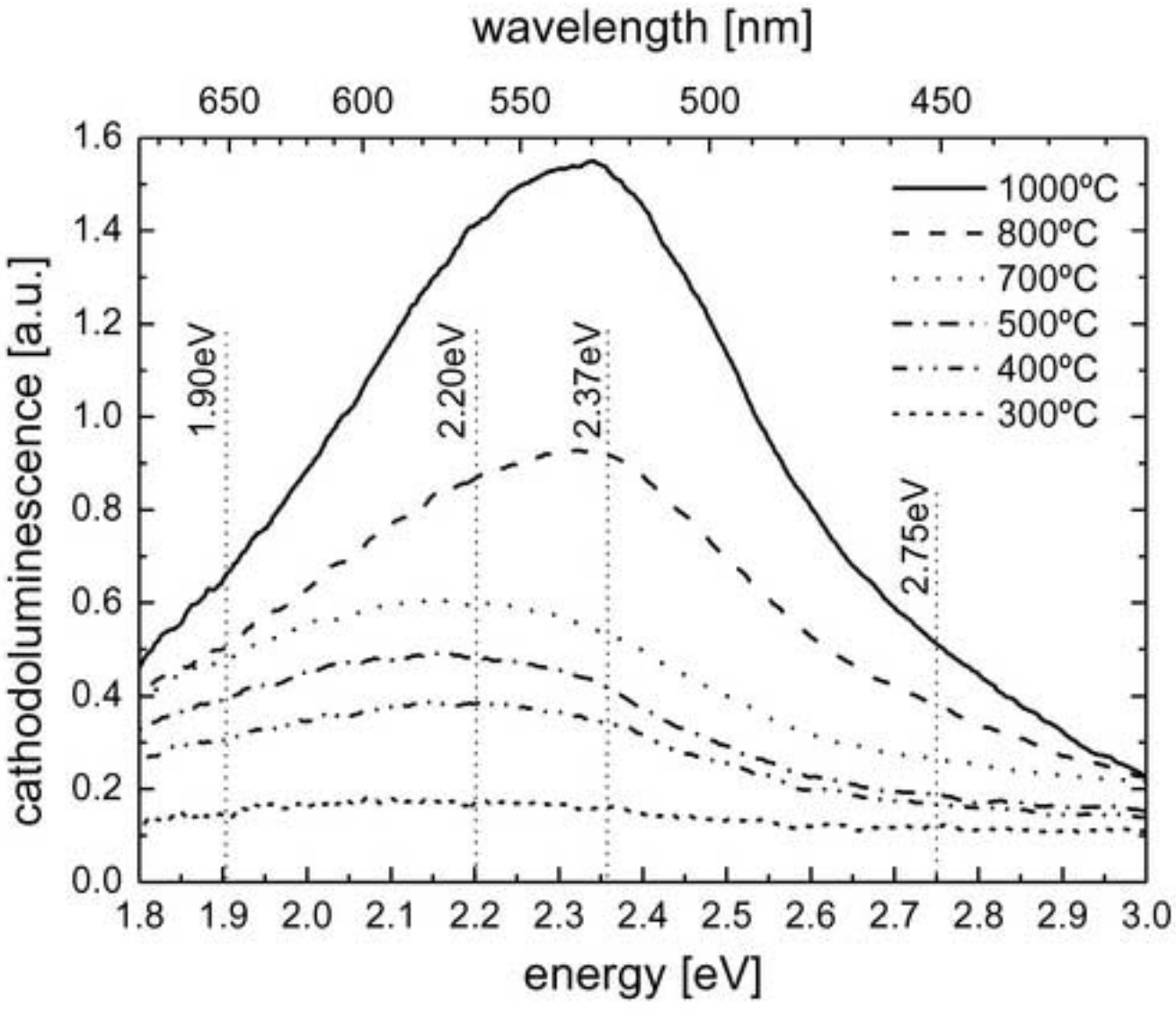

Figure 3

Click here to download high resolution image

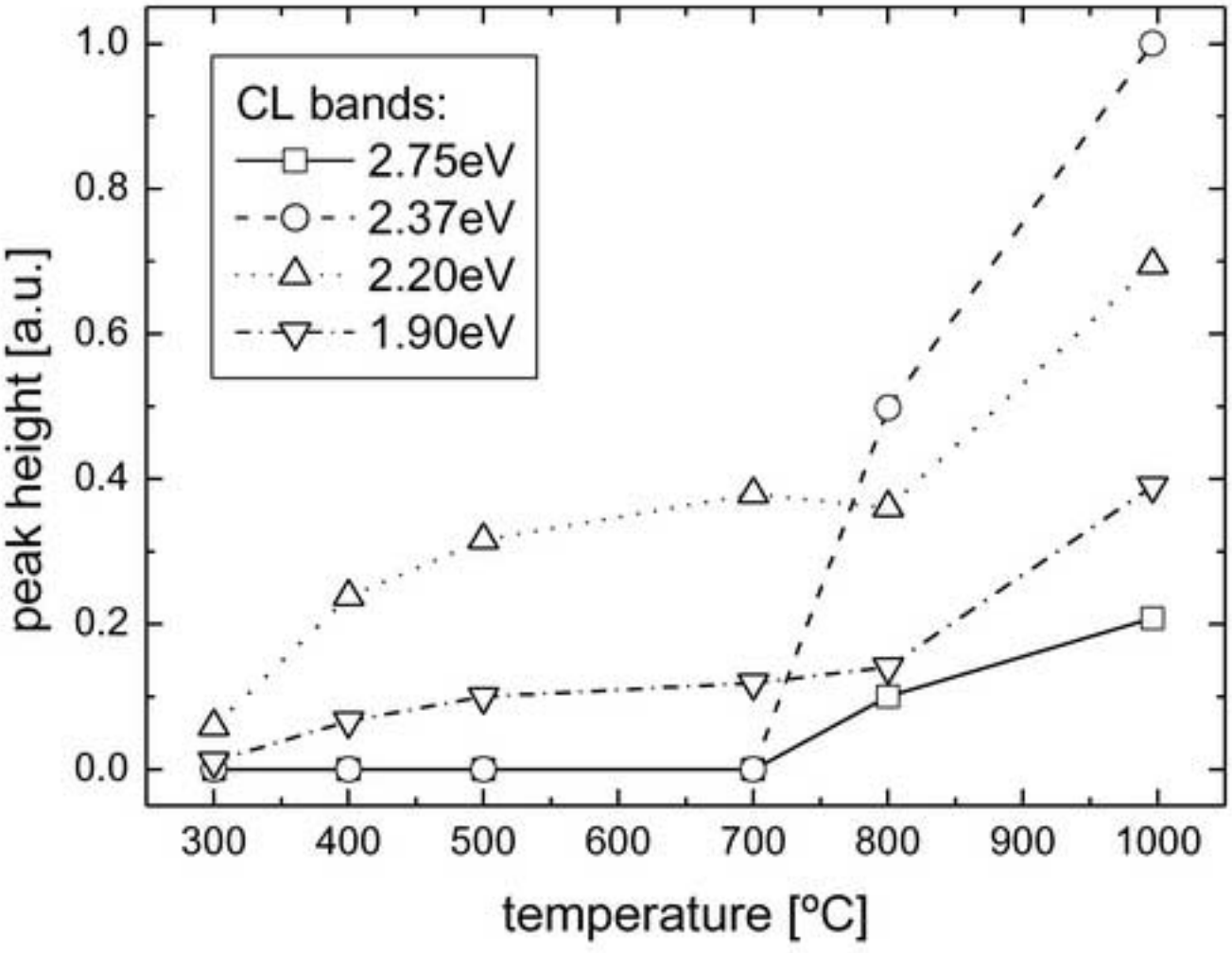

Figure 4

Click here to download high resolution image

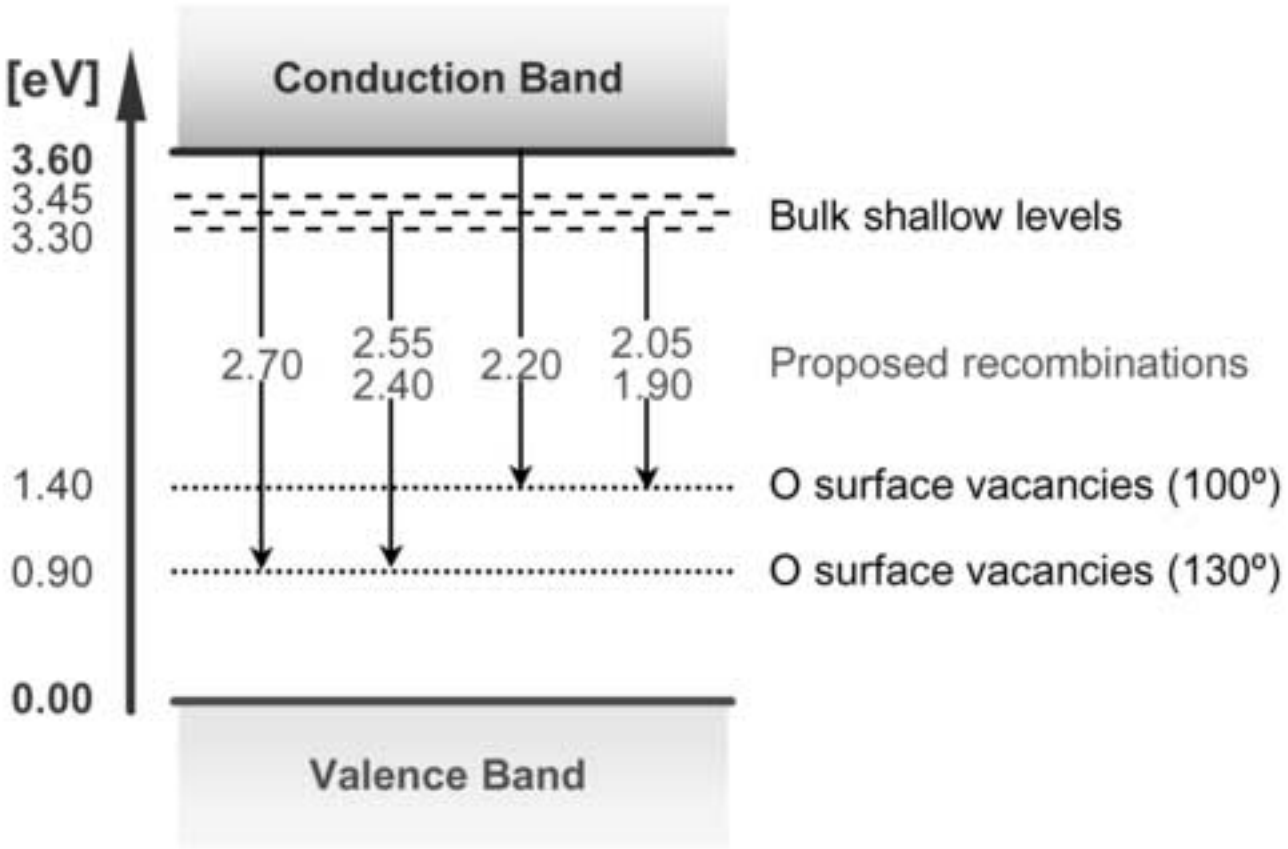

Figure 5

Click here to download high resolution image

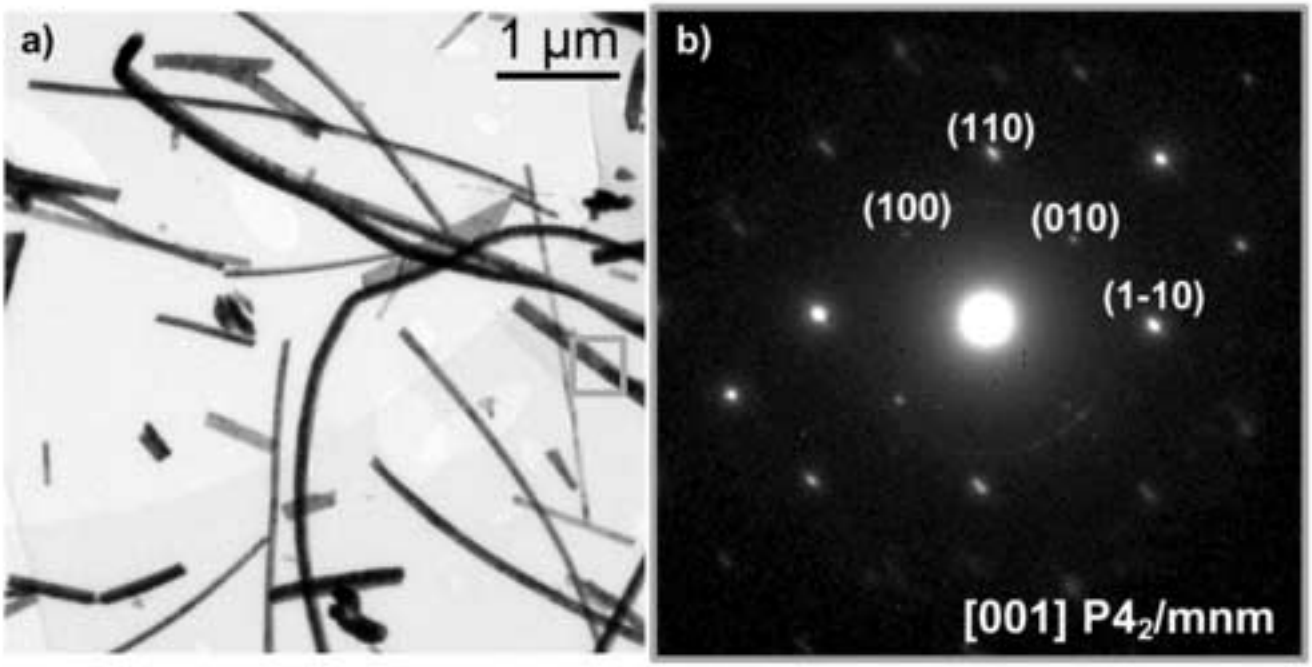

Figure 6

Click here to download high resolution image

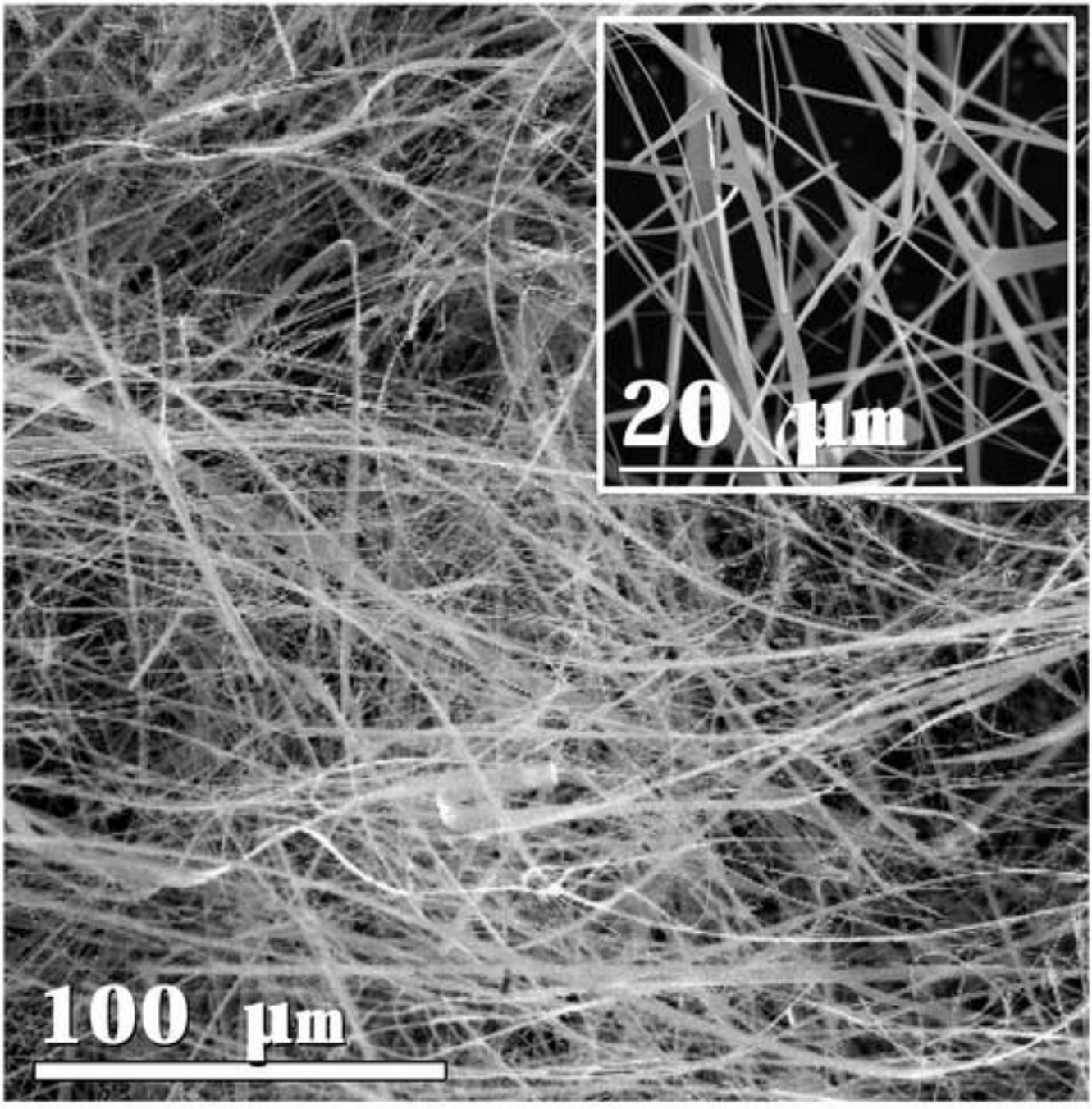

Figure 7

Click here to download high resolution image